Along-stream transport and transformation of dissolved organic matter in a large tropical river

Thibault Lambert[1,*], Cristian R. Teodoru[2], Frank C. Nyoni[3], Steven Bouillon[2], François Darchambeau[1], Philippe Massicotte[4] and Alberto V. Borges[1].

[1] University of Liège, Chemical Oceanography Unit, Liège, Belgium

[2] KU Leuven, Department of Earth and Environmental Sciences, Leuven, Belgium

[3] University of Zambia, Integrated Water Resources Management Center, Lusaka, Zambia

[4] Aarhus University, Department of Bioscience, Denmark

* Corresponding author

Abstract - Large rivers transport considerable amounts of terrestrial dissolved organic matter (DOM) to the ocean. However, downstream gradients and temporal variability in DOM fluxes and characteristics are poorly studied at the scale of large river basins, especially in tropical areas. Here, we report longitudinal patterns in DOM content and composition based on absorbance and fluorescence measurements along the Zambezi River and its main tributary, the Kafue River, during two hydrological seasons. During high flow periods, a greater proportion of aromatic and humic DOM was mobilized along rivers due to the hydrological connectivity with wetlands, while low flow periods were

characterized by lower DOM content of less aromaticity resulting from loss of connectivity with wetlands, more efficient degradation of terrestrial DOM and enhanced autochthonous productivity. Changes in water residence time due to contrasting water discharge were found to modulate the fate of DOM along the river continuum. Thus, high water discharge promotes the transport of terrestrial DOM downstream relative to its degradation while low water discharge enhances the degradation of DOM during its transport. The longitudinal evolution of DOM was also strongly impacted by a hydrological buffering effect in large reservoirs in which the seasonal variability of DOM fluxes and composition was strongly reduced.

1. Introduction

The composition, transport and transformation of dissolved organic matter (DOM) in large rivers are key aspects for determining regional and global carbon (C) budgets (Schlesinger and Melack, 1981), the fate of terrigenous DOM flowing to the oceans (del Giorgio and Pace, 2008; Massicotte and Frenette, 2011), the influence of fluvial inputs on DOM biogeochemistry in coastal and oceanic environments (Holmes et al., 2008), and the functioning of inland waters as active pipes with regards to the global C cycle (Cole et al., 2007; Borges et al., 2015a). Riverine DOM is mainly derived from terrestrial soils (e.g. Weyhenmeyer et al., 2012), but can also be fueled by sources within the aquatic system (Lapierre and Frenette, 2009; Massicotte and Frenette, 2011). Longitudinal patterns of riverine DOM, both in terms of concentration and composition, are controlled by numerous environmental drivers including connectivity with surrounding wetlands (Battin, 1998; Mladenov et al., 2007), lateral inputs from tributaries (Massicotte and Frenette, 2011) and shifts in dominant land cover (Ward et al., 2015). Once in the aquatic ecosystem, terrestrial DOM is exposed to in-stream processing such as photodegradation (Cory et al., 2007;

48 Spencer et al., 2009), microbial respiration (Amon and Benner, 1996; Fasching et al.,
49 2014), and flocculation (von Wachenfeldt and Tranvik, 2008), that usually operate
50 simultaneously and lead to the removal and the transformation of DOM during its transport
51 (Massicotte and Frenette, 2011; Cawley et al., 2012). The composition of DOM has been
52 identified as a major driver determining its reactivity in freshwaters (Weyhenmeyer et al.,
53 2012; Kothawala et al., 2014; Kellerman et al., 2015). For example, the selective loss of
54 the colored fraction of terrestrial DOM is a common pattern observed in a wide variety of
55 ecosystems (Moran et al., 2000; Cory et al., 2007; Spencer et al., 2009; Weyhenmeyer et
56 al., 2012). However, aquatic ecosystem properties (e.g., temperature, oxygen availability
57 or composition of aquatic microbial community) may also play an equal role in determining
58 the fate of DOM (Marín-Spiotta et al., 2014). Thus, the extent of DOM decay depends on
59 the water residence time (WRT) of the aquatic ecosystem (Cory et al., 2007; Hanson et
60 al., 2011; Köhler et al., 2013). In large rivers, WRT varies spatially, increasing in reservoirs
61 and lakes compared to river channels, and seasonally, being higher during low flow
62 compared to high flow. Considering that changes in water level also control the
63 hydrological connectivity with wetlands, it is likely that the downstream gradient in DOM
64 composition drastically differs in relation to spatial and temporal changes in hydrodynamic
65 conditions.

66 Longitudinal patterns of DOM in large rivers are often assessed in one specific
67 environment, such as wetlands/floodplains (Mladenov et al., 2007; Yamashita et al., 2010;
68 Cawley et al., 2012; Zurbrügg et al., 2013) or lakes (Parks and Baker, 1997; Massicotte
69 and Frenette 2013; Stackpoole et al., 2014), or limited to a subsection of large rivers (del
70 Giorgio and Pace; 2008; Massicotte and Frenette, 2011; Ward et al., 2015), and mostly
71 carried out during one specific hydrological period. Our understanding of rivers as a

continuum in which DOM is simultaneously transported from terrestrial soils to oceans, produced and degraded is thus fundamentally limited by a lack of basin-scale studies taking into account seasonal variations. This is especially true for tropical waters that have the highest riverine dissolved organic carbon (DOC) flux to the oceans (Meybeck, 1993) but for which DOM cycling has received less attention than rivers in other climate zones with the exception of the Amazon River (Mayorga et al., 2005; Johnson et al., 2011; Ward et al., 2013; 2015).

The study of DOM biogeochemistry at large spatial and temporal scales requires analytical tools that are simple to implement but have a large sample throughput while providing pertinent information about the DOM chemical composition. Spectroscopic methods, primarily based on ultraviolet-visible and fluorescence measurements, fulfill these criteria (Jaffé et al., 2008). Optical properties of colored DOM (CDOM) and fluorescent DOM (FDOM) can be used to calculate several indices related to DOM composition. These include the specific ultraviolet absorbance at 254 nm ($SUVA_{254}$), positively related to the degree of DOM aromaticity (Weishaar et al., 2003), the spectral slope ratio (S_R), inversely related to the average DOM molecular weight (Helms et al., 2008) and the fluorescence index (FI), related to the contribution of terrestrial versus aquatic microbial inputs (McKnight et al., 2001). FDOM measurements acquired as three-dimensional excitation-emission matrices (EEMs) and coupled with the parallel factor analysis (PARAFAC) provide additional benefits for the characterization of DOM (Stedmon et al., 2003; Stedmon and Markager, 2005; Yamashita et al., 2008). In addition, the carbon stable isotope composition of DOC ($\delta^{13}C_{DOC}$) can provide information about the terrestrial or aquatic origin of DOM (Mladenov et al., 2007; Lambert et al., 2015).

The Zambezi River basin, the fourth largest river in Africa, was extensively sampled from its source to its mouth during three field campaigns carried out over wet and dry seasons (Teodoru et al., 2015; Fig. 1 and 2). Longitudinal patterns of DOM were assessed through measurements of DOC concentrations and characterization of DOM ($\delta^{13}C_{DOC}$ coupled with CDOM and FDOM) along the Zambezi River (>3000 km) and its main tributary, the Kafue River (>1500 km). The aim of this study was to determine the main drivers on downstream patterns of DOM at the scale of a large tropical river, with a specific attention to the role of WRT in modulating the fate of DOM.

2. Materials and methods

2.1. Study site. The Zambezi River has a drainage area of 1.4×10^6 km², originates in northwestern Zambia and flows southeast over 3000 km before it discharges into the Indian Ocean in Mozambique (Fig. 1). The climate of the Zambezi Basin is classified as humid subtropical and is characterized by two main seasons, the rainy season from October/November to April/May and the dry season from May/June to September/October. Annual precipitation strongly varies with latitude, from > 2000 mm in the northern part and around Lake Malawi to less than 500 mm in the southern part of the basin. The mean annual rainfall over the entire catchment is ~940 mm (Chenje, 2000). Up to 95% of the annual rainfall occurs during the rainy period while the dry period presents irregular and sporadic rainfall events. Consequently, water discharge in Zambezi River has a unimodal distribution with a single maximum peak discharge occurring typically in April/May and a minimum in November (Fig. 2).

Woodlands and shrublands are the dominant (55%) land cover and stretch over the whole catchment; forests (20%) and grasslands (9%) areas are mainly confined to the

118 northeast part of the basin and croplands represents 13% of the total area (Mayaux et al.,
119 2004). Wetlands, including swamps, marshes, seasonally inundated floodplains and
120 mangroves cover 5% of the total basin area (Lehner and Döll, 2004).

121 Based on distinct geomorphological characteristics, the Zambezi Basin can be divided
122 into three major segments: (1) the upper Zambezi from the headwaters to Victoria Falls;
123 (2) the middle Zambezi, from Victoria Falls to the edge of the Mozambique coastal plain
124 (below Cahora Bassa Gorge); and (3) the lower Zambezi, the stretch crossing the coastal
125 plain down to the Indian Ocean (Wellington, 1955). The upper Zambezi covers about 40%
126 of the total area of the Zambezi basin but comprises the highest fraction of wetlands and
127 floodplains (about 60% of the total wetlands/floodplains areas of the Zambezi Basin),
128 including the Barotse Floodplain and the Chobe Swamps (Fig. 1). The middle stretch of
129 the Zambezi River is buffered by two major man-made impoundments, namely the Kariba
130 Reservoir (volume: 167 km³; area: 5364 km² (Magadza, 2010)) and the Cahora Bassa
131 Reservoir (volume: 63 km³; area: 2739 km² (Davies et al., 2000)). The Kafue River
132 (drainage area: 1.56×10^5 km²) joins the Zambezi River ~ 70 km downstream of the Kariba
133 Dam. Similarly to the upper Zambezi, the Kafue River comprises a high density of
134 wetlands/floodplains (about 26% of the total wetlands/floodplains areas of the Zambezi
135 basin), including the Lukanga Swamps and the Kafue Flats (Fig. 1). It also comprises two
136 smaller reservoirs, the Itezhi Tezhi Reservoir (volume: 5.4 km³; area: 365 km² (Kunz et
137 al., 2011)) and the Kafue Gorge Reservoir (volume: ~1 km³; area: 13 km² (Teodoru et al.,
138 2015)). In its lower part, the Zambezi River and its tributary the Shire River both drain
139 narrow but ~ 200 km long wetlands areas before their confluence zone. At the end of its
140 course, the river forms a large, 100 km long floodplain-delta system of swamps and
141 meandering channels.

142 **2.2. Sampling and analytical methods.** Sampling was conducted during two
143 consecutive years and over two climatic seasons: wet season 2012 (1 February to 5 May,
144 n=40), wet season 2013 (6 January to 21 March, n=41), and dry season 2013 (15 October
145 to 28 November, n=24) (Fig. 2). Sites in the Zambezi and the Kafue rivers were located
146 100 – 150 km apart from the spring to the outlet (Fig. 1) except during the 2013 dry season
147 when sampling in the Zambezi River ended before its entrance in the Cahora Bassa
148 Reservoir due to logistical constraints.

149 Water sampling was mainly performed from boats or dugout canoes in the middle
150 of the river. In few case (n=10), in the absence of boats/canoes, sampling was carried out
151 either from bridges or directly from the shore and as far as possible away from the
152 shoreline, but without discernable effects on the longitudinal patterns on DOM or other
153 biogeochemical variables (Teodoru et al., 2015). Approximately 2 L of water were
154 collected 0.5 m below the surface, kept away from direct sunshine and filtered within 2 h
155 of sampling. The samples preparation for the different analysis was performed just after
156 filtrations. Filtrations were performed successively on pre-combusted GF/F glass fiber
157 filters (0.7 µm porosity), then on 0.2 µm polyethersulfone syringe filters. Samples for the
158 measurement of DOC concentration and $\delta^{13}C_{DOC}$ signatures were stored in 40 mL glass
159 vials with polytetrafluoroethylene (PTFE) coated septa with 50 µL H_3PO_4 (85%). Samples
160 for CDOM/FDOM analyses were stored in 20 mL amber glass vials with PTFE-coated
161 septa but without H_3PO_4 addition. Samples for major elements (including Fe) were stored
162 in 20 mL scintillation vials and acidified with 50 µl of HNO_3 (65 %) prior to analysis.
163 Samples were brought back to Belgium for analysis. For logistical reasons, it was not
164 possible to store the samples cold, but the effects of room temperature storage over

several months on samples collected using our preservation technique has been found to preserve both DOC, $\delta^{13}C_{DOC}$, and CDOM properties (own unpublished results).

2.3. DOC analysis. DOC and $\delta^{13}C_{DOC}$ were analyzed with an Aurora1030 total organic carbon analyzer (OI Analytical) coupled to a Delta V Advantage isotope ratio mass spectrometer (KU Leuven, Belgium). Typical precision observed in duplicate samples was in >95% cases < ± 5 % for DOC, and ± 0.2 ‰ for $\delta^{13}C_{DOC}$. Quantification and calibration was performed with series of standards prepared in different concentrations, using both IAEA-C6 ($\delta^{13}C$ = -10.4 ‰) and in-house sucrose standards ($\delta^{13}C$=-26.9 ‰). All data are reported in the δ notation relative to VPDB (Vienna Pee Dee Belemnite).

2.4. CDOM analysis and calculations. Absorbance was recorded on a Perkin-Elmer UV/Vis 650S spectrophotometer (Université Libre de Bruxelles) using a 1 cm quartz cuvette. Absorbance spectra were measured between 190 and 900 nm at 1 nm increment and instrument noise was assessed measuring ultrapure (Type 1) Milli-Q (Millipore) water as blank. After subtracting the blank spectrum, the correction for scattering and index of refraction was performed by fitting the absorption spectra to the data over the 200-700 nm range according to the following equation:

$$A_\lambda = A_0 e^{-S(\lambda-\lambda_0)} + K \quad (1)$$

where A_λ and A_0 are the absorbance measured at defined wavelength λ and at reference wavelength λ_0 = 375 nm, respectively, S the spectral slope (nm^{-1}) that describes the approximate exponential decline in absorption with increasing wavelength and K a background offset. The fit was not used for any purpose other than to provide an offset value K that was then subtracted from the whole spectrum (Lambert et al., 2015).

The $SUVA_{254}$ was calculated as the UV absorbance at λ = 254 nm (A_{254}) normalized to the corresponding DOC concentration (Weishaar et al., 2003). The natural UV

absorbance of Fe at λ = 254 nm was estimated based on measured Fe concentrations and was then subtracted from the UV absorbance measured. The corrected value of A_{254} was then used to calculate $SUVA_{254}$. The $SUVA_{254}$ was used as an indicator of the aromaticity of DOC with high values (>3.5 l mgC^{-1} m^{-1}) indicating of the presence of more complex aromatic moieties and low values (<3 l mgC^{-1} m^{-1}) indicative of the presence of more aliphatic compounds (Weishaar et al., 2003).

Napierian absorption coefficients were calculated according to:

$$a_\lambda = 2.303 \times A_\lambda / L \quad (3)$$

where a_λ is the absorption coefficient (m^{-1}) at wavelength λ, A_λ the absorbance corrected at wavelength λ and L the path length of the optical cell in m (0.01 m). CDOM was reported as the absorption coefficient at 350 nm (a_{350}). Spectral slopes for the intervals 275-295 nm and 350-400 nm were determined from the linear regression of the log-transformed *a* spectra versus wavelength. The slope ratio S_R was calculated as the ratio of $S_{275-295}$ to $S_{350-400}$ according to Helms et al. (2008). S_R is related to the molecular weight distribution of DOM with values less than 1 indicative of enrichment in high molecular weight compounds and high values above 1 indicative of a high degree of low molecular weight compounds (Helms et al., 2008).

2.5. FDOM analysis and PARAFAC modeling. Fluorescence intensity was recorded on a Perkin-Elmer LS55 fluorescence spectrometer (Université Libre de Bruxelles) using a 1 cm quartz cuvette across excitation wavelengths of 220-450 nm (5 nm increments) and emission wavelengths of 230-600 nm (0.5 nm increments) in order to build excitation–emission matrices (EEMs). If necessary, samples were diluted until A_{254} < 0.2 m^{-1} to avoid problematic inner filter effects (Ohno, 2002). Before each measurement session (i.e. each day), a Milli-Q water sample was also analysed. EEMs preprocessing such as removing

first and second Raman scattering, standardization to Raman units, absorbance corrections and inner filter effects were performed prior the PARAFAC modelling. The scans were standardized to Raman units (normalized to the integral of the Raman signal between 390 nm and 410 nm in emission at a fixed excitation of 350 nm) with a Milli-Q water sample run the same day as the samples (Zepp et al., 2004). PARAFAC model was build using MATLAB (MathWorks, Natick, MA, USA) and DOM Fluorescence Toolbox 1.7. Validation of the PARAFAC model was performed by split-half analysis and random initialization (Stedmon and Bro, 2008). Additional samples analysed in the same manner and collected from (1) tributaries of the Zambezi and the Kafue rivers as well as during an almost two-year monitoring period of the Zambezi and the Kafue rivers (n = 42; data not published), and (2) the Congo Basin (n = 164; data not published) were added to the dataset. This was done to increase the variability of DOM fluorescence signatures and therefore help detect components that could have been present in insufficient quantity to be detected in our environment (Stedmon and Markager, 2005). The maximum fluorescence F_{Max} values of each component for a particular sample provided by the model were summed to calculate the total fluorescence signal F_{Tot} of the sample in Raman's unit (R.U.). The relative abundance of any particular PARAFAC component X was then calculated as $\%C_X = F_{Max}(X)/ F_{Tot}$. The FI index was calculated as the ratio of the emission intensities at 470 nm and 520 nm at an excitation wavelength of 370 nm (McKnight et al., 2001). A higher FI value (e.g., 1.8) indicates an aquatic microbial DOM source while a lower value (e.g., 1.2) indicates a terrestrial source; intermediate values indicate a mixed DOM source.

2.6. Statistical Analysis

A principal component analysis (PCA) was initially used as a diagnostic tool to examine relationships between PARARAC results, DOM concentration and composition assessed by optical proxies and isotopic measurements in order to better characterize the origin and source of the PARAFAC components identified in the study. The PCA was performed on scaled variables using the prcomp function in R software. DOC concentrations, stable carbon isotopic composition, optical indices ($SUVA_{254}$, S_R, FI), a_{350}, F_{Max} and the relative abundance of PARAFAC components were used as the variables for the PCA. Given the different units of the variables used in the PCA, data were scaled to zero-mean and unit-variance as recommended (Borcard et al., 2011). The PCA was then performed on the correlation matrix of the scaled variables.

3. Results

3.1. Longitudinal patterns in DOC concentration, composition and DOM optical properties

Data were acquired during two wet seasons and one dry season. The two wet season datasets are discussed together hereafter. DOC concentrations in the Zambezi River ranged from 1.9 ± 0.1 to 4.9 ± 1.0 mg L^{-1} during the wet periods and from 1.2 to 2.9 mg L^{-1} during the dry period (Fig. 3A). Along the upper Zambezi DOC increased downstream during the wet seasons, while DOC gradually decreased downstream during the dry season. In the Kariba Reservoir, DOC variability between wet and dry seasons was relatively low, and concentrations ranged from 2.4 ± 0.3 to 2.9 ± 1.4 mg L^{-1}. DOC exhibited relatively small variability downstream of the Kariba Reservoir and along the lower Zambezi, with the exception of a slight increase during the wet seasons downstream of the confluence with the Shire River (outlet of Lake Malawi). In the Kafue River, DOC

was generally higher during the wet seasons (from 3.1 ± 0.1 to 5.4 ± 0.7 mg L^{-1}) compared to the dry season (from 1.3 to 3.6 mg L^{-1})(Fig. 3B). Despite this seasonal difference, DOC increased gradually downstream during both wet and dry seasons. DOC concentrations in the Itezhi Tezhi Reservoir showed a decrease (~25%) during the wet seasons but an increase (~20%) during the dry season compared to the upstream station. During the wet periods, DOC concentrations in the upper Zambezi and the Kafue River were closely correlated with the extent of wetlands (Fig. 4).

The a_{350} values (Fig. 3C and 3D), used to assess the level of CDOM, were higher during the wet seasons (1.7 to 16.6 m^{-1} in the Zambezi and 3.9 to 11.5 m^{-1} in the Kafue) than during the dry season (1.3 to 10.7 m^{-1} in the Zambezi and 1.2 to 4.7 m^{-1} in the Kafue). They followed similar spatial and seasonal patterns as DOC concentrations, with some differences. First, decreases in a_{350} values were more pronounced than for DOC, especially in the upper Zambezi during the dry season and in the Kariba and Itezhi Tezhi reservoirs during the wet season. For example, while DOC decreased by a factor ~2 as the Zambezi enters the Kariba Reservoir during the wet periods, a_{350} decreased by a factor ~4. Secondly, while DOC concentrations were higher at the outlet of reservoirs compared to upstream stations during the dry season, a_{350} values were lower.

$\delta^{13}C_{DOC}$ values in the Zambezi basin ranged from -28.1 to -19.6 ‰ over the study period, i.e. from typical C_3 dominated values (C_3 end-member was estimated at -28.5 ‰ according to Kohn(2010) to values representing mixed C_3-C_4 vegetation($\delta^{13}C$ value for the C_4 end-member -12.1 ‰ (Tamooh et al., 2012)). $\delta^{13}C_{DOC}$ showed a gradual increase along the Zambezi River during all periods, from -28.1 and -26.5 ‰ at the source to -21.4 to -20.1 ‰ near its delta, the latter being especially marked between the two first sampling

sites in the upper Zambezi (Fig. 3E), while no significant pattern was observed along the Kafue River (values between -25.9 and -20.5 ‰, Fig. 3F).

DOM at the source of the Zambezi exhibited the highest $SUVA_{254}$ (> 4 L mgC^{-1} m^{-1}, indicating strong aromaticity), and lowest S_R (< 0.8, indicative high molecular weight) values during both wet and dry seasons (Fig. 3G and 3I). During the wet seasons, the upper Zambezi was characterized by stable $SUVA_{254}$ (3.5 – 4.0 L mgC^{-1} m^{-1}) and low S_R (0.85 – 0.91) values. In the middle Zambezi, $SUVA_{254}$ and S_R values were lowest (2.2 ± 0.2 – 2.9 ± 0.1 L mgC^{-1} m^{-1}) and highest (1.22 ± 0.09 – 1.41 ± 0.01) in the Kariba and the Cahora Bassa reservoirs compared to samples collected in-between (2.6 ± 0.1 – 3.1 ± 0.02 L mgC^{-1} m^{-1} for $SUVA_{254}$ and 0.97 ± 0.1 – 1.10 ± 0.08 for S_R). Overall, $SUVA_{254}$ increased from 2.1±0.5 to 2.9±0.9 L mgC^{-1} m^{-1} whereas S_R decreased from 1.08±0.09 to 0.97±0.04 in the lower Zambezi, with maximum (3.3±0.9 L mgC^{-1} m^{-1}) and minimum (0.88±0.006) values recorded below the confluence with the Shire River, respectively. During the wet periods, FI values ranged between 1.24 and 1.41 in the mainstream, and between 1.43 and 1.58 in reservoirs (Fig. 3K). FI values during the dry season were generally higher than during the wet periods with values ranging from 1.29 to 1.72, except at the source of the Zambezi, where an FI value of 1.19 was observed.

In the Kafue River, variations in DOM composition were marked between the wet and dry seasons, but minimal along the longitudinal transect (Fig. 3H, 3J and 3L). $SUVA_{254}$ and S_R ranged from 3.5 to 4.0 L mgC^{-1} m^{-1} and from 0.79 to 1.05, respectively, during the wet seasons, except in the Itezhi Tezhi Reservoir where $SUVA_{254}$ decreased to 2.4 L mgC^{-1} m^{-1} and S_R increased up to 1.16. Values were quite stable during dry periods, and ranged between 2.2 and 2.8 L mgC^{-1} m^{-1} for $SUVA_{254}$ and from 1.11 to 1.22 for S_R. FI values

ranged between 1.27 and 1.42 during the wet seasons, and between 1.41 and 1.74 during the dry season.

3.2. Longitudinal patterns in FDOM

PARAFAC modelling identified three terrestrial humic-like components (C1, C2 and C4), one aquatic microbial humic-like component (C3) and one protein tryptophan-like (C5) component (Table 1 and Supplementary Fig. 1). In the Zambezi River, the fluorescence intensities (F_{Max}) of PARAFAC components during the wet seasons presented patterns similar to DOC concentrations with some exceptions (Fig. 5). F_{Max} of the C4 component presented the higher percentage of increase compared to the other component in river sections flowing through wetlands/floodplains in the upper and lower Zambezi (data not shown). All terrestrial and microbial humic-like components showed a systematic and marked decrease in their F_{Max} values in reservoirs, while F_{Max} of C5 decreased in a smaller proportion in the Kariba Reservoir and increased in the Cahora Bassa Reservoir. During the dry season, F_{Max} of terrestrial humic-like components decreased downstream concurrent with DOC concentrations, while F_{Max} remained stable for C3 or increased for C5. In the Kafue River, F_{Max} of all components followed similar spatial and temporal patterns as those of DOC concentrations. The main difference observed was that while F_{Max} values of humic-like compounds were lower during the dry season compared to the wet seasons, F_{Max} of C5 exhibited similar values accross the hydrological cycle.

As a direct consequence of the spatial and temporal differences in F_{Max} of PARAFAC components, the relative contribution of each component to the total fluorescence signal F_{TOT} showed distinct patterns (Fig. 6). Thus, the downstream decrease of %C1 and %C2 observed in the upper Zambezi during the wet seasons can

be related to the parallel increase of %C4, the latter being due to the more pronounced increase in F_{Max} of C4 relative to the other components. The same patterns for %C1 and %C2 observed during the dry season, however, reflect the fact that F_{Max} values of C3 and C5 were stable or increased during the dry season, respectively, while F_{Max} of C1 and C2 decreased. %C5 was higher during the dry season compared to the wet seasons, and reached highest values in reservoirs during the wet periods due to its specific spatial and temporal variations in F_{Max} values. No longitudinal changes in the relative abundance of PARAFAC components were observed along the Kafue River. Similar to what was observed along the Zambezi River, the dry season was marked by a decrease in %C4 and an increase in %C5, while %C1, %C2 and %C3 were equivalent to values recorded during the wet seasons.

3.3. Principal component analysis (PCA)

The first two components of the PCA explained 71.7% of the variance and regrouped the variables in three main clusters (Fig. 7). The first includes %C1, %C2 and samples collected at or near the source of the Zambezi. The second group was defined by %C4 and several variables including DOC, F_{Max}, $SUVA_{254}$ and a_{350}. Samples from the upper Zambezi and from the Kafue rivers (excluding reservoirs) were mainly located in this cluster. Finally, %C3 and %C5 were clustered with S_R and FI. Samples from reservoirs (including Kariba, Cahora Bassa and Itezhi Tezhi) were almost all in this cluster. Samples collected in the middle and lower Zambezi during both the wet and dry seasons were located between the distinct clusters defined by PARAFAC components and DOM concentration and composition.

4. Discussion

352 **4.1. Identification of PARAFAC components**. Humic-like components C1 and C2 are
353 among the most common fluorophores found in freshwaters and are associated with high
354 molecular weight and aromatic compounds of terrestrial origin (Stedmon and Markager,
355 2005; Yamashita et al., 2008; Walker et al., 2013). Component C4 has been reported to
356 be of terrestrial origin (Stedmon and Markager, 2005; Kothawala et al., 2015) or to be a
357 photoproduct of terrestrially derived DOM (Massicotte and Frenette, 2011). The
358 association of %C4 with DOC concentrations and terrestrial optical indices including a_{350}
359 and $SUVA_{254}$ advocates for a terrestrial origin of this component (Fig. 7). Conversely, %C3
360 and %C5 were negatively correlated with a_{350} and $SUVA_{254}$. C3 and C5 components are
361 respectively classified as microbial humic-like and tryptophan-like components related to
362 the production of DOM within aquatic ecosystems (Kothawala et al., 2014; Kellerman et
363 al., 2015). Both fluorophores can originate from autochthonous primary production
364 (Yamashita et al., 2008; 2010; Lapierre and Frenette, 2009) or from degradation of
365 terrestrial DOM in the water column as previously reported in a wide variety of
366 environments as marine (Jørgensen et al., 2011) and lake waters (Kellerman et al., 2015)
367 for C3, and large Arctic rivers (Walker et al., 2013) or small temperate catchment (Stedmon
368 and Markager, 2005) for C5. The opposite relationship of %C1 and %C2 versus %C3 (Fig.
369 7) suggests that C3 would be the result of the transformation of terrestrial components C1
370 and C2 through biological activity in the water column as suggested by Jørgensen et al.
371 (2011). The distribution of samples along PC1 is thus likely controlled by the transition
372 from terrestrial DOM with a high degree of aromaticity and humic content (negative
373 loadings) to less aromatic DOM produced within the aquatic ecosystem by the degradation
374 of terrestrial DOM during transport and/or by autochthonous sources (positive loadings).
375 Regarding PC2, %C1 and %C2 were also strongly opposed to $\delta^{13}C_{DOC}$. Considering the

highest level of %C1 and %C2 at the source of the Zambezi and suggesting that $\delta^{13}C_{DOC}$ was primarily controlled by the vegetation gradient along the mainstem from C_3 forest toward mixed C_3/C_4 savannah, this suggests that land cover influences DOM in the river network.

4.2. Relative contribution of C_3 and C_4 plants to the DOM pool. The $\delta^{13}C_{DOC}$ values in the Zambezi basin were in the range of data reported for other African river systems, being higher than those measured in C_3 tropical rainforest catchments such as the Congo (Spencer et al., 2009; Bouillon et al., 2012, 2014), the Ogooué (Lambert et al., 2015) or the Nyong rivers (Brunet et al., 2009), but similar to catchments with significant areas of C_4 vegetation (e.g. savannah) such as the Tana (Tamooh et al., 2012), the Niger (Lambert et al., 2015) or the Betsiboka and Rianilia rivers (Marwick et al., 2014).

The increase in $\delta^{13}C_{DOC}$ in the Zambezi, especially marked along the first stations, was consistent with the vegetation gradient along the mainstem, where upstream C_3 forest ecosystems quickly shift towards mixed C_3-C_4 grassland and woodland/shrubland ecosystems that dominate in the basin (Supplementary Fig. 2). $\delta^{13}C_{DOC}$ did not show marked depletion in surface waters of reservoirs, suggesting that phytoplankton production had little net effect on $\delta^{13}C_{DOC}$ (Bouillon et al., 2009; Tamooh et al., 2012). In addition to an increased contribution from C_4 vegetation, the downstream increase in $\delta^{13}C_{DOC}$ could also partially result from differences in the $\delta^{13}C$ composition of C_3 vegetation at the basin scale. Indeed, $\delta^{13}C$ values of C_3 plants increase with decreasing mean annual precipitation (MAP) (Kohn, 2010) and MAP in the Zambezi strongly varies from > 2000 mm yr^{-1} in the northern part of the basin to < 500 mm yr^{-1} in the southern part (Chenje, 2000). Using high resolution maps of MAP (Hijmans et al., 2005), a digital elevation model at 3 arcsec resolution computed by the HydroSHEDS mapping product

400 (http://hydrosheds.cr.usgs.gov/index.php), and the proposed equation of Kohn (2010) that
401 estimates the $\delta^{13}C$ signature of C_3 vegetation based on MAP, altitude and latitude, we
402 estimated an average value of -27.1 ‰ and a range of variation from -29.3 to -26.0 ‰ for
403 the C_3 vegetation of the Zambezi basin (Supplementary Fig. 3). This shift of 3.3% is
404 smaller than the observed shift of ~8 % in the Zambezi River, indicating that the increase
405 of $\delta^{13}C_{DOC}$ is to a large extent due to increased contribution from C_4 vegetation. As a first
406 approximation and using values of -27.1 ‰ for C_3 plants (calculated above) and -12.1 ‰
407 for C_4 plants (Tamooh et al., 2012), we found that DOM in the Zambezi basin was mainly
408 from C_3 origin, with a relative contribution of ~69% and ~75 % for DOC during the wet and
409 dry period, respectively.

410 **4.3. Seasonal and spatial variability in downstream gradients in DOM concentration**
411 **and composition.** Altogether data showed clear changes in the downstream gradients of
412 DOM concentration and composition, both seasonally and spatially. In addition to the
413 vegetation gradient, these changes were essentially controlled by three main factors:
414 WRT and connectivity with wetlands/floodplains, both highly dependent on seasonal
415 variations in water level (and discharge), and water retention by lakes/reservoirs that is
416 more independent from seasonal variations of water level.

417 **4.3.1 Land cover and hydrological connectivity with wetlands/floodplains.** The DOM
418 at the source of the Zambezi was clearly distinct from the rest of the basin, independently
419 of the hydrological period (Fig. 6), with a strong aromatic character (highest $SUVA_{254}$), a
420 high degree of molecules with elevated molecular weight (lowest S_R) and low $\delta^{13}C_{DOC}$.
421 The shift in land cover (see Supplementary Fig. 2) was reflected in the DOM gradient from
422 the source station of the Zambezi to the next sampling site, and marked by an increase in
423 S_R, $\delta^{13}C_{DOC}$ and a decrease in $SUVA_{254}$. This pattern is consistent with the role of forest

424 in releasing more aromatic DOM of high molecular weight than other vegetation types in
425 tropical freshwaters (Lambert et al., 2015).

426 Downstream, the variability in the optical properties of DOM between wet and dry
427 seasons indicated seasonal changes in the sources of riverine DOM in relation with
428 changes in water level and connectivity with wetlands/floodplains. The high $SUVA_{254}$ and
429 low S_R values during the wet seasons indicate the mobilisation of fresh aromatic DOM of
430 high molecular weight due to the increased water flow through DOM-rich upper soil
431 horizons during high flow periods (Striegl et al., 2005; Neff et al., 2006; Mann et al., 2012;
432 Bouillon et al., 2014). Wetlands and floodplains were the main sources of terrestrial DOM
433 at the basin scale during wet seasons, as shown by the relationships between DOC and
434 wetland extent (Fig. 4). Among the different terrestrial humic-like components, C4 was the
435 most affected by fluctuations in the connectivity with wetlands/floodplains. The increase
436 in the relative contribution of C4 suggests that this component was mobilized in greater
437 proportion relative to others (Fig. 6). This observation is consistent with a recent study
438 conducted in boreal streams, in which a component similar to C4 was found to increase
439 relative to other humic-like fluorophores (equivalent to C1 and C2) in stream waters during
440 the peak spring melt due to the higher abundance of this component in uppermost soil
441 horizons of wetlands (Kothawala et al., 2015). The longitudinal and seasonal variations in
442 %C4 in the upper Zambezi are consistent with the hypothesis that C4 is mainly produced
443 in the upper soil horizons of wetlands/floodplains and therefore preferentially mobilized
444 during high flow periods.

445 **4.3.2 WRT modulates the downstream patterns of DOM.** During the dry season, DOM
446 was characterized by lower $SUVA_{254}$ and higher S_R values, indicating the transport of
447 compounds of lower aromaticity and lower average molecular weight compared to high

448 flow periods. The difference in downstream gradients of DOM compared to the wet
449 seasons can be explained in part by the loss of connectivity between rivers and riparian
450 wetlands/floodplains and the deepening of hydrological flowpaths through DOM-poor
451 deeper subsoil horizons during the dry season (e.g. Striegl et al., 2005; Bouillon et al.,
452 2014). Changes of connectivity with wetland during the dry season was also found to
453 strongly impact CO_2 and CH_4 distribution in the Zambezi (Teodoru et al., 2015). That being
454 said, the considerable decrease in water discharge during dry/base flow period compared
455 to wet/high flow periods (Fig. 2) likely leads to a decrease in water velocities and
456 subsequently to an increase in water residence time, allowing a more efficient degradation
457 of terrestrial DOM along a given section. For illustration, the preferential downstream loss
458 of a_{350} compared to DOC in the upper Zambezi, associated with a gradual decrease of
459 $SUVA_{254}$ and increase of S_R, is a strong evidence of the preferential loss of the terrestrial
460 and aromatic fraction of DOM through photodegradation (e.g. Spencer et al., 2009;
461 Weyhenmeyer et al., 2012). The stable level of F_{Max} of C3 suggests a continuous supply
462 of this component, likely due to microbial degradation of terrestrial DOM. In addition, the
463 increase in WRT could favour the accumulation of DOM from autochthonous sources as
464 suggested by higher values of FI and the gradual increase in F_{Max} for C5 (Fig. 3 and 4).
465 Flushing during high flow periods perturbs the downstream gradient of DOM established
466 during base flow because (1) increasing water level mobilizes a greater proportion of
467 terrestrial DOM and (2) higher water velocities increases the travel distance of humic and
468 aromatic terrestrial compounds before removal due to microbial and photochemical
469 degradation processes and limits the accumulation of autochthonous DOM in the water
470 column.

4.3.3. Retention of water by lakes/reservoirs. Longitudinal patterns of DOM were affected by the presence of reservoirs where DOM was characterized by low aromaticity and molecular weight and higher microbial contribution independently of water level fluctuations (Fig. 5 and 7). The net loss of DOC and the preferential loss of the coloured and aromatic fraction of DOM (based on a_{350} and $SUVA_{254}$, Fig. 3) in lakes and reservoirs have been previously documented (Hanson et al., 2011; Köhler et al., 2013) and attributed to the combination of several processes including flocculation, photochemical and microbial degradation (Cory et al., 2007; von Wachenfeldt and Tranvik, 2008; Köhler et al., 2013; Kothawala et al., 2014). Although we were not able to estimate the relative contribution of these mechanisms, our results indicate that the humic-like fractions of DOM (C1-C4) were more susceptible to degradation compared to the protein-like fraction (C5), an observation consistent with recent studies carried out in boreal lakes (Kothawala et al., 2014). The level of fluorescence of C5 could be additionally sustained by the FDOM from primary producers such as macrophytes (Lapierre and Frenette, 2009) or phytoplankton (Yamashita et al., 2008), that also lead to low values of the partial pressure of CO_2 below atmospheric equilibrium in the Kariba and Cahora Bassa reservoirs while rivers (i.e., excluding reservoirs) displayed CO_2 supersaturated conditions with respect to atmospheric equilibrium (Teodoru et al., 2015).

In agreement with others studies (e.g. Hanson et al., 2011), the effects of reservoirs on the fate of DOM were related to their specific WRT. The Itezhi Tezhi Reservoir had little effect on longitudinal patterns of DOM, as also suggested by a recent study (Zürbrugg et al., 2013), likely due to its relatively low WRT (0.7 yr, Kunz et al., 2011) compared to the Kariba (5.7 yr, Magadza, 2010) and the Cahora Bassa (~2 yr, Davies et al., 2000)

494 reservoirs. The DOC concentrations upstream and downstream of the Cahora Bassa
495 Reservoir were similar but DOM composition exhibited significant changes within the
496 reservoir compared to upstream and downstream stations, suggesting a balance between
497 loss and production of new compounds. In fact, the Kariba Reservoir was the most
498 important reservoir responsible for the perturbation of the longitudinal DOM gradient. The
499 seasonal variability of DOM at the outlet of the Kariba Reservoir, both in terms of
500 concentration and composition, was drastically reduced compared to the seasonal
501 patterns observed in the upper Zambezi (Fig. 3 and 5). This was also illustrated by data
502 from an almost two-year monitoring of the Zambezi River 70 km downstream of the Kariba
503 Dam, showing that the terrestrial fraction of DOM leaving the reservoir has undergone
504 extensive transformation (Table 2). The role of lakes/reservoirs in lowering the seasonality
505 of DOC in river network has also been evidenced in temperate and boreal streams and
506 rivers in Sweden (Winterdahl et al., 2014).
507 Beyond their role as hotspots for DOM processing and mineralization,
508 lakes/reservoirs act as a hydrological buffer and reduce the temporal variability of
509 downstream water flow (Goodman et al., 2011; Lottig et al. 2013). Except for some
510 isolated events, water discharge remained constant at Kariba Dam due to hydropower
511 management (Fig. 2). Combined with the low temporal variability in DOM content (Table
512 2), DOC fluxes at the outlet of the Kariba Reservoir were relatively invariant and ranged
513 between 8.3×10^7 and 9.7×10^7 kg yr^{-1}. This results in a twofold decrease of DOC fluxes
514 during the wet seasons between upstream inputs from the upper Zambezi and export at
515 the outlet of the Kariba Reservoir, but in the increase by a factor of 12 during the dry
516 season (Fig. 8). On a longitudinal perspective, lakes/reservoirs can thus shift from DOM
517 sources to sinks relative to upstream ecosystems while reducing the temporal variation of

518 DOM fluxes and composition to downstream ecosystems. That being said, DOM losses
519 were largely offset during the wet seasons by inputs from the Kafue and the Shire rivers
520 as well as from wetlands in the lower Zambezi (Fig. 3 and 8). Therefore, the spatial
521 arrangement of the different elements that constitute large river networks such as
522 lakes/reservoirs, wetlands/floodplains and large tributaries is a key aspect in controlling
523 DOM export at the basin scale.

524 **4.4. Comparison with others rivers.** The results of this study are similar to those
525 reported in large rivers from other biomes regarding (1) the role of peak flow periods in
526 exporting a greater portion of terrestrial aromatic and humic DOM (Neff et al., 2006; Duan
527 et al., 2007; Holmes et al., 2008; Walker et al., 2013; Bouillon et al., 2014), (2) the
528 disproportionate importance of riparian wetlands and floodplains in regulating in-stream
529 chemistry (Fiebig et al. 1990; Dosskey and Bertsch, 1994; Hinton et al. 1998; Battin, 1998;
530 Hanley et al., 2013; Abril et al., 2014; Borges et al., 2015b) and (3) the reactivity of
531 terrestrial DOM during its transport (Massicotte and Frenette, 2011; Cawley et al., 2012;
532 Wehenmeyer et al., 2012). However, while changes in temperature have been suggested
533 as a secondary factor impacting DOM patterns in temperate and boreal streams and rivers
534 (Kothawala et al., 2014; Winterdahl et al., 2014; Raymond et al., 2015), changes in
535 longitudinal DOM patterns in the Zambezi Basin were only controlled by changes in
536 hydrology. Indeed, water temperatures were systematically elevated with values mainly
537 ranging from 25 to 29°C (data not shown) and no significant patterns were apparent
538 between the contrasting seasons.

539 Our study clearly illustrates that the DOC in a given station is the legacy of
540 upstream sources and their degree of processing during transport, and suggests that WRT
541 is a major driver controlling the fate of DOM in freshwaters (the latter resulting from the

competition between transport and degradation processes). Seasonal changes in DOM concentration and composition in large rivers assessed by monitoring programs are often explained by vertical changes in DOM sources mobilized during high flow and base flow conditions, i.e. shallow versus deep sources along the soil profile (Neff et al., 2006; Mann et al., 2012; Bouillon et al., 2014). Our results show that the upstream degradation history of DOM during transit should also be taken into consideration, especially during base flow periods. Given the strong reactivity of fresh terrestrial humic DOM exported during high flow periods (e.g. Holmes et al., 2008; Mann et al., 2012) and the ability of large hydrological events to transport DOM downstream over large distances (Raymond et al., 2015), the functioning of large rivers at the seasonal scale and their impacts on receiving ecosystems (e.g. coastal waters) should deserve more attention.

Author contributions

The research project was designed by AVB and SB, field data collection was done by CRT and FCN. CDOM and FDOM measurements were done by TL with the help of FD. Data analysis was done by TL with the help of PM for PARAFAC modelling. Manuscript was drafted by TL and was commented, amended and approved by all co-authors.

Acknowledgements

This work was funded by the European Research Council (ERC-StG 240002 AFRIVAL), the Fonds National de la Recherche Scientifique (FNRS, FluoDOM J.0009.15), and the Research Foundation Flanders (FWO-Vlaanderen, travel grants to CRT). We thank Christiane Lancelot (Université Libre de Bruxelles) for access to the Perkin-Elmer UV/Vis 650S and two anonymous reviewers for constructive comments on the previous version

565 of the manuscript. TL is a postdoctoral researcher at the FNRS. AVB is a senior research
566 associate at the FNRS.

567 **Supplementary Information** accompanies this paper.

568

569 **References**

570 Abril, G., Martinez. J. M., Artigas, L. F., Moreira-Turcq. P., Benedetti, M. F., 5 Vidal, L.,
571 Meziane, T., Kin, J. H., Bernardes, M. C., Savoye, N., Deborde, J., Souza, E. L.,
572 Albéric, P., Landim de Souza, M. F., and Roland, F.: Amazon River carbon dioxide
573 outgassing fuelled by wetlands, Nature, 505, 395–398, doi:10.1038/nature12797,
574 2014.

575 Amon, R. M. W. and Benner, R.: Bacterial utilization of different size classes of dissolved
576 organic matter, Limnol. Oceanogr., 41, 41–51, 1996.

577 Battin, T. J.: Dissolved organic matter and its optical properties in a blackwater tributary
578 of the upper Oricono river, Venezuela, Org. Geochem., 28, 561-569,1998.

579 Borcard, D., Gillet, F., and Legendre, P.: Numerical ecology with R, Springer New York,
580 New York, 306 pp., doi.org/10.1007/978-1-4419-7976-6, 2011.

581 Borges, A. V., Darchambeau, F., Teodoru, C. R., Marwick, T. R., Tamooh, F.,
582 Geeraert, N., Omengo, F. O., Guerin, F., Lambert, T., Morana, C., Okuku, E.,
583 and Bouillon, S.: Globally significant greenhouse-gas emissions from african
584 inland waters, Nature Geosci., 8, 637-642, doi:10.1038/ngeo2486, 2015a.

585 Borges, A. V., Abril, G., Darchambeau, F., Teodoru, C. R., Deborde, J., Vidal, L. O.,
586 Lambert, T., and Bouillon, S.: Divergent biophysical controls of aquatic CO_2 and CH_4
587 in the World's two largest rivers; Sci. Rep., 5, 15614, doi: 10.1038/srep15614, 2015b.

588 Bouillon, S., Abril, G., Borges, A. V., Dehairs, F., Govers, G., Hughes, H. J., Merckx, R.,
589 Meysman, F. J. R., Nyunja, J., Osburn, C., and Middelburg, J. J.: Distribution, origin
590 and cycling of carbon in the Tana River (Kenya): a dry season basin-scale survey
591 from headwa- ters to the delta, Biogeosciences, 6, 2475–2493, doi:10.5194/bg-6-
592 2475-2009, 2009.
593 Bouillon, S., Yambélé, A., Gillikin, D. P., Teodoru, C. R., Darchambeau, F., Lambert, T.,
594 and Borges, A. V.: Contrasting biogeochemical characteristics of the Oubangui River
595 and tributaries (Congo River basin), Sci. Rep., 4, 1–10, doi:10.1038/srep05402,
596 2014.
597 Brunet, F., Dubois, K., Veizer, J., Nkoue Ndondo, G. R., Ndam Ngoupayou, J. R., Boeglin,
598 J. L., and Probst, J. L.: Terrestrial and fluvial carbon fluxes in a tropical watershed:
599 Nyong basin, Cameroon, Chem. Geol., 265, 563–572, 2009.
600 Cawley, K. M., Wolski, P., Mladenov, N., and Jaffé, R.: Dissolved organic matter
601 biogeochemistry along a transect of the Okavango delta, Bostwana, Wetlands, 32,
602 475–486, doi: 10.1007/s13157-012-0281-0, 2012.
603 Chenje, M.: State of the Environment Zambezi Basin 2000, SADC, IUCN, ZRA, and
604 SARDC, Maseru, Lusaka and Harare, 334 pp., ISBN 978-1-77910-009-2, 2000.
605 Cole, J. J., Prairie, Y. T., Caraco, N. F., McDowell, W. H., Tranvik, L. J., Striegl, R. G.,
606 Duarte, C. M., Kortelainen, P., Downing, J. A., Middelburg, J. J., and Melack, J.:
607 Plumbing the global carbon cycle: integrating inland waters into the terrestrial carbon
608 budget, Ecosystems, 10, 171–184, 2007.
609 Cory, R. M., McKnight, D. M., Chin, Y. P., Miller, P., and Jaros, C. L.: Chemical
610 characteristics of fulvic acids from Arctic surface waters: Microbial contributions and

611 photochemical transformations, J. Geophys. Res.-Biogeosci., 112, G04S51,
612 doi:10.1029/2006JG000343, 2007.
613 Davies, B. R., Beilfuss, R. D., and Thoms, M. C.: Cahora Bassa retrospective, 1974-1997:
614 effects of flow regulation on the lower Zambezi River, Verh. Int. Ver. Theor. Angew.,
615 20, 2149–2157, 2000.
616 del Giorgio, P. A. and Pace, M. L.: Relative independence of dissolved organic carbon
617 transport and processing in a large temperate river: the Hudson River as both pipe
618 and reactor, Limnol. Oceanogr., 53, 185-197, 2008.
619 Dosskey, M. G. and Bertsch, P. M.: Forest sources and pathways of organic matter
620 transport to a blackwater stream: a hydrologic approach, Biogeochemistry, 24, 1-19,
621 1994.
622 Duan, S., Bianchi, T. and Sampere, T. P.: Temporal variability in the composition and
623 abundance of terrestrially-derived dissolved organic matter in the lower Mississippi
624 and Pearl Rivers, Mar. Chem., 103, 172–184, doi:10.1016/j.marchem.2006.07.003,
625 2007.
626 Fasching, C., Behounek, B., Singer, G. A., and Battin, T. J.: Microbial degradation of
627 terrigenous dissolved organic matter and potential consequences for carbon cycling
628 in brown-water streams, Scientific reports, 4, doi:10.1038/srep04981, 2014.
629 Fiebig, D. M., Lock, M. A., and Neal, C.: Soil water in the riparian zone as a source of
630 carbon for a headwater stream, J. Hydrol., 116, 217-237, 1990.
631 Goodman, K. J., Baker, M. A., and Wurtsbaugh, W. A.: Lakes as buffers of stream
632 dissolved organic matter (DOM) variability: temporal patterns of DOM characteristics
633 in mountain stream-lake systems, J. Geosphys. Res., 116, G00N02,
634 doi:10.1029/2011JG001709, 2011.

635 Hanley, K., Wollheim, W. M., Salisbury, J., Huntington, T., and Aiken, G.: Controls on
636 dissolved organic carbon quantity and chemical character in temperate rivers of
637 North America, Global Biogeochem. Cycles, 27, 492–504, doi:10.1002/gbc.20044,
638 2013.
639 Hanson, P. C., Hamilton, D. P., Stanley, E. H., Preston, N., Langman, O. C., and Kara, E.
640 L.: Fate of allochthonous dissolved organic carbon in lakes: a quantitative approach,
641 PLoS ONE, 6, e21884, doi:10.1371/journal.pone.0021884, 2011.
642 Helms, J. R., Stubbins, A., Ritchie, J. D., Minor, E. C., Kieber, D. J., and Mopper, K.:
643 Absorption spectral slopes and slope ratios as indicators of molecular weight,
644 source, and photobleaching of chromophoric dissolved organic matter, Limnol.
645 Oceanogr., 53, 955–969, 2008.
646 Hijmans, R .J., Cameron, S. E, Parra, J. L., Jones, P.G., and Jarvis, A.: Very high
647 resolution interpolated climate surfaces for global land areas. Int. J. Climatol., 25,
648 1965-1978, 2005.
649 Hinton, M. J., Schiff, S. L., and English, M. C.: Sources and flow- paths of dissolved
650 organic carbon during storms in two forested watershed of the Precambrian Shield,
651 Biogeochemistry, 41, 175– 197, 1998.
652 Holmes, R. M., McClelland, J. W., Raymond, P. A., Frazer, B. B., Peterson, B. J., and
653 Stieglitz, M.: Lability of DOC transported by Alaskan rivers to the arctic ocean,
654 Geophys. Res. Lett., 35, 5, L03402, doi:10.1029/2007gl032837, 2008.
655 Jaffé, R., McKnight, D., Maie, N., Cory, R., McDowell, W. H., and Campbell, J. L.: Spatial
656 and temporal variations in DOM composition in ecosystems: The importance of long-
657 term monitoring of optical properties, J. Geophys. Res.-Biogeo., 113, G04032,
658 doi:10.1029/2008jg000683, 2008.

659 Johnson, M S., Couto, E. G. Abdo, M., and Lehmann, J.: Fluorescence index as an
660 indicator of dissolved organic carbon quality in hydrologic flowpaths of forested
661 tropical watersheds, Biogeochemistry, 105, 149-157, doi: 10.1007/s10533-011-
662 9595-x, 2011.
663 Jørgensen, L., Stedmon, C. A., Kragh, T., Markager, S., Middelboe, M., and Søndergaard,
664 M.: Global trends in the fluorescence characteristics and distribution of marine
665 dissolved organic matter, Mar. Chem., 126, 139–148, doi:
666 10.1016/j.marchem.2011.05.002, 2011.
667 Kellerman, A. M., Kothawala, D. N., Dittmar, T., and Tranvik, L. J.: Persistence of
668 dissolved organic matter in lakes related to its molecular characteristics, Nat.
669 Geosci., 8, 454–457, doi: 10.1038/ngeo2440, 2015.
670 Köhler, S. J., Kothawala, D., Futter, M. N., Liungman, O., and Tranvik, L.: In-lake
671 processes offset increased terrestrial inputs of dissolved organic carbon and color in
672 lakes, PLoS ONE, 8, e70598, doi:10.1371/journal.pone.0070598, 2013.
673 Kohn, J. M.: Carbon isotope compositions of terrestrial C3 plants as indicators of
674 (paleo)ecology and (paleo)climate, P. Natl. Acad. Sci. USA, 107, 19691–19695,
675 2010.
676 Kothawala, D. N., Ji, X., Laudon, H., Ågren, A., Futter, M. N., Köhler, S. J., and Tranvik,
677 L. J.: The relative influence of land cover, hydrology, and in-stream processing on
678 the composition of dissolved organic matter in boreal streams, J. Geosphys. Res-
679 Biogeo., 120, 1491–1505, doi: 10.1002/2015JG002946, 2015.
680 Kothawala, D. N., Stedmon, C. A., Müller, R. A., Weyhenmeyer, G. A., Köhler, S. J., and
681 Tranvik, L. J.: Controls of dissolved organic matter quality: Evidence from a large-

682 scale boreal lake survey, Glob. Change Biol., 20, 1101–1114,
683 doi:10.1111/gcb.12488, 2014.
684 Kunz, M. J., Wuest, A., Wehrli, B., Landert, J., and Senn, D. B.: Impact of a large tropical
685 reservoir on riverine transport of sediment, carbon and nutrients to downstream
686 wetlands, Water Resour. Res., 47, W12531, doi:10.1029/2011WR010996, 2011.
687 Lambert, T., Darchambeau, F., Bouillon, S., Alhou, B., Mbega, J- D, Teodoru, C. R., Nyoni,
688 F. C., and A V Borges, A. V.: Landscape control on the spatial and temporal
689 variability of chromophoric dissolved organic matter and dissolved organic carbon in
690 large African rivers, Ecosystems, 18, 1224–1239, doi:10.1007/s10021-015-9894-5,
691 2015.
692 Lapierre, J. F. and Frenette, J. J.: Effects of macrophytes and terrestrial inputs on
693 fluorescent dissolved organic matter in a large river system, Aquat. Sci., 71, 15–24,
694 doi:10.1007/s00027-009-9133-2, 2009.
695 Lehner, B. and Döll, P.: Development and validation of a global database of lakes,
696 reservoirs and wetlands, J. Hydrol., 296, 1–22, doi:10.1016/j.jhydrol.2004.03.028,
697 2004.
698 Lottig, N. R., Buffam, I., and Stanley, E. H.: Comparisons of wetland and drainage lake
699 influences on stream dissolved organic concentrations and yields in a north
700 temperate lake-rich region, Aquat. Sci., 75, 619–630, doi: 10.1007/s00027-013-
701 0305-8, 2013.
702 Magadza, C.: Environmental state of Lake Kariba and Zambezi River Valley: Lessons
703 learned and not learned. Lakes & Reservoirs: Research & Management, 15, 167–
704 192, doi:10.1111/j.1440-1770.2010.00438.x, 2010.

Mann, P. J., Davydova, A., Zimov, N., Spencer, R. G. M., Davydov, S., Bulygina, E., Zimov, S. and Holmes, R. M.: Controls on the composition and lability of dissolved organic matter in Siberia's Kolyma River basin, J. Geosphys. Res., 117, G01028, doi:10.1029/2011JG001798, 2012.

Marín-Spiotta, E., Gruley, K. E., Crawford, J., Atkinson, E. E., Miesel, J. R., Greene, S., Cardona-Correa, C., and Spencer, R. G. M.: Paradigm shifts in soil organic matter research affect interpretations of aquatic carbon cycling: transcending disciplinary and ecosystem boundaries, Biogeochemistry, 117, 279-297, doi: 10.1007/s10533-013-9949-7, 2014.

Marwick, T., Borges, A. V., Van Acker, K., Darchambeau, F., and Bouillon, S.: Disproportionate Contribution of Riparian Inputs to Organic Carbon Pools in Freshwater Systems, Ecosystems, 17, 974–989, 2014.

Massicotte, P. and Frenette, J.-J.: Spatial connectivity in a large river system: resolving the sources and fate of dissolved organic matter, Ecol. Appl., 21, 2600–2617, 2011.

Mayaux, P., Bartholomé, E., Fritz, S., and Belward, A.: A new land-cover map of Africa for the year 2000, J. Biogeogr., 31, 861–877, 2004.

Mayorga, E., Aufdenkampe, A. K., Masiello, C. A., Krusche, A. V., Hedges, J. I., Quay, P. D., Richey, J. E., and Brown, T. A.: Young organic matter as a source of carbon dioxide outgassing from Amazonian rivers, Nature, 436, 538–541, doi:10.1038/nature03880, 2005.

McKnight, D. M., Boyer, E. W., Westerhoff, P. K., Doran, P. T., Kulbe, T., and Andersen, D. T.: Spectrofluorometric characterization of dissolved organic matter for indication of precursor organic material and aromaticity, Limnol. Oceanogr., 46, 38–48, 2001.

728 Meybeck, M.: Riverine transport of atmospheric carbon: source, global typology and
729 budget. Water, Air, and Soil Pollution, 70, 443–463, 1993.
730 Mladenov, N, McKnight, D. M., Macko, S. A., Norris, M., Cory, R. M., and Ramberg, L.:
731 Chemical characterization of DOM in channels of a seasonal wetland, Aquat. Sci.,
732 69, 456–471, doi:10.1007/s00027-007-0905-2, 2007.
733 Moran, M. A., Sheldon, W. M., and Zepp, R. G.: Carbon loss and optical property changes
734 during long-term photochemical and biological degradation of estuarine dissolved
735 organic matter, Limnol. Oceanogr., 45, 1254–1264, 2000.
736 Neff, J. C., Finlay, J. C., Zimov, S. A., Davydov, S. P., Carrasco, J. J., Schuur, E. A. G.,
737 and Davydova, A. I.: Seasonal changes in the age and structure of dissolved organic
738 carbon in Siberian rivers and streams Geophy. Res. Lett., 33, L23401,
739 doi:10.1029/2006GL028222, 2006.
740 Ohno, T.: Fluorescence inner-filtering correction for determining the humification index of
741 dissolved organic matter, Environ. Sci. Technol., 36, 742–746,
742 doi:10.1021/Es0155276, 2002.
743 Parks, S. J. and Baker, L. A.: Sources and transport of organic carbon in an Arizona river-
744 reservoir system, Wat. Res., 31, 1751–1759, 1997.
745 Raymond, P. A., Saiers, J. E., and Sobczak W. V.: Hydrological and biogeochemical
746 controls on watershed dissolved organic matter transport: pulse-shunt concept,
747 Ecology, in press, doi.org/10.1890/14-1684.1, 2015.
748 Schlesinger, W. H. and Melack, J. M.: Transport of organic carbon in the world's rivers,
749 Tellus, 33, 172-187, 1981.
750 Spencer, R. G. M., Stubbins, A., Hernes, P. J., Baker, A., Mopper, K., Aufdenkampe, A.
751 K., Dyda, R. Y., Mwamba, V. L., Mangangu, A. M., Wabakanghanzi, J. N., and Six,

752 J.: Photochemical degradation of dissolved organic matter and dissolved lignin
753 phenols from the Congo River, J. Geophys. Res.-Biogeo., 114,
754 doi:10.1029/2009jg000968, 2009.
755 Stackpoole, S. M., Stets, E. G., and Striegl, R. G.: The impact of climate and reservoirs
756 on longitudinal riverine carbon fluxes from two major watersheds in the Central and
757 Intermontane West, J. Geosphys. Res-Biogeo., 119, 848–863, doi:
758 10.1002/2013JG002496, 2014.
759 Stedmon, C. A. and Markager, S.: Resolving the variability in DOM fluorescence in a
760 temperate estuary and its catchment unsing PARAFAC, Limnol.Oceanogr, 50, 686–
761 697, 2005.
762 Stedmon, C. A. and Bro, R.: Characterizing dissolved organic matter fluorescence with
763 parallel factor analysis: a tutorial, Limnol. Oceanogr. Meth., 6, 572–579, 2008.
764 Stedmon, C. A., Markager, S., and Bro, R.: Tracing dissolved organic matter in aquatic
765 environments using a new approach to fluorescence spectroscopy, Mar. Chem., 82,
766 239–254, doi:10.1016/s0304-4203(03)00072-0, 2003.
767 Striegl, R. S., Aiken, G. R., Domblaser, M. M., Raymond, P. A., and Wickland, K. P.: A
768 decrease in discharge-normalized DOC export by the Yukon River during summer
769 through autumn, Geophy. Res. Lett., 32, L21413, doi:10.1029/2005GL024413,
770 2005.
771 Tamooh, F., Van den Meersche, K., Meysman, F., Marwick, T. R., Borges, A. V., Merckx,
772 R., De- hairs, F., Schmidt, S., Nyunja, J., and Bouillon, S.: Distribution and origin of
773 suspended matter and organic carbon pools in the Tana River Basin, Kenya,
774 Biogeosciences, 9, 2905–2920, doi:10.5194/bg-9-2905-2012, 2012.

775 Teodoru, C. R., Nyoni, F. C., Borges, A. V., Darchambeau, F., Nyambe, I., and Bouillon,
776 S.: Dynamics of greenhouse gases (CO_2, CH_4, N_2O) along the Zambezi River and
777 major tributaries, and their importance in the riverine carbon budget,
778 Biogeosciences, 12, 2431–2453, doi:10.5194/bg-12-2431-2015, 2015.
779 von Wachenfekdt, E. and Tranvik, L. J.: Sedimentation in Boreal lakes - the role of
780 flocculation of allochthonous dissolved organic matter in the water column.
781 Ecosystems 11, 803–814, doi: 10.1007/s10021-008-9162-z, 2008.
782 Walker, S. A., Amon, R. M., and Stedmon, C. A.: Variations in high-latitude riverine
783 fluorescent dissolved organic matter: A comparison of large Arctic rivers, J.
784 Geosphys. Res-Biogeo., 118, 1689–1702, doi:10.1002/2013JG002320, 2013.
785 Ward, N. D., Keil, R. G., Medeiros, P. M., Brito, D. C., Cunha, A. C., Dittmar, T., Yager, P.
786 L., Krusche, A. V., and Richey, J. E.: Degradation of terrestrially derived
787 macromolecules in the Amazon River, Nat. Geosci., 6, 530–533,
788 doi:10.1038/ngeo1817, 2013.
789 Ward, N. D., Krusche, A. V., Sawakuchi, H. O., Brito, D. C., Cunha, A. C., Moura, J. M.
790 S., da Silva, R., Keil, R. G., and Richey, J. E.: The compositional evolution of
791 dissolved and particulate organic matter along the lower Amazon River-Óbidos to
792 the ocean, Mar. Chem., 177, 244–256, doi.org/10.1016/j.marchem.2015.06.013,
793 2015.
794 Weishaar, J. L., Aiken, G. R., Bergamaschi, B. A., Fram, M. S., Fujii, R., and Mopper, K.:
795 Evaluation of specific ultraviolet absorbance as an indicator of the chemical
796 composition and reactivity of dissolved organic carbon, Environ. Sci. Technol., 37,
797 4702–4708, doi: 10.1021/es030360x, 2003.

798 Wellington, J. H.: Southern Africa – a Geographic Study, vol. 1, Physical Geography,
799 Cambridge University Press, Cambridge, 528 pp., 1955.
800 Weyhenmeyer, G. A., Fröberg, M., Karltun, E., Khalili, M., Kothawala, D., Temnerud, J.,
801 and Tranvik, L. J.: Selective decay of terrestrial organic carbon during transport from
802 land to sea, Glob. Change Biol., 18, 349–355, doi:10.1111/j.1365-
803 2486.2011.02544.x, 2012.
804 Winterdahl, M., Erlandsson, M., Futter, M. N., Weyhenmeyer, G. A., and Bishop, K.: Intra-
805 annual variability of organic carbon concentrations in running waters: Drivers along
806 a climatic gradient, Global Biogeochem. Cycles, 28, 451-464,
807 doi:10.1002/2013GB004770, 2014.
808 Yamashita, Y., Jaffé, R., Maie, N. and Tanoue, E.: Assessing the dynamics of dissolved
809 organic matter (DOM) in coastal environments by excitation emission matrix
810 fluorescence and parallel factor analysis (EEM-PARAFAC), Limnol. Oceanogr., 53,
811 1900–1908, 2008.
812 Yamashita, Y., Scinto, L. J., Maie, N., and Jaffé, R.: Dissolved organic matter
813 characteristics across a subtropical wetland's landscape: application of optical
814 properties in the assessment of environmental dynamics, Ecosystems, 13, 1006–
815 1019, doi:10.1007/s10021-010-9370-1, 2010.
816 Zepp, R. G., Sheldon, W. M., and Moran, M. A.: Dissolved organic fluorophores in
817 southeastern US coastal waters: correction method for eliminating Rayleigh and
818 Raman scattering peaks in excitation–emission matrices, Mar. Chem., 89, 15–36,
819 doi:10.1016/j.marchem.2004.02.006, 2004.

820 Zurbrügg, R., Suter, S., Lehmann, M. F., Wehrli, B., and Senn, D. B.: Organic carbon and
821 nitrogen export from a tropical dam-impacted floodplain system, Biogeosciences, 10,
822 23–38, doi: 10.5194/bg-10-23-2013, 2013.
823

824 **Figure captions**

825 **Figure 1 –** Map of the Zambezi basin showing elevation, wetlands and floodplains areas
826 (data from Lehner and Döll, 2004), the main hydrological network and the distribution of
827 sampling sites along the Zambezi and the Kafue rivers.

828 **Figure 2 –** Water discharge between January 2012 and January 2014 for (a) the Zambezi
829 River at Victoria Falls and at Kariba Dam, and (b) for the Kafue River at Hook Bridge
830 located upstream of the Itezhi Tezhi Reservoir and at the Kafue Gorge Dam (data from
831 Zambia Electricity Supply Corporation Limited, ZESCO). Bars refer to the three periods
832 during which field campaigns were performed.

833 **Figure 3 –** Longitudinal variations of DOM properties along the Zambezi River (left panels)
834 and the Kafue River (right panels) during the wet and the dry seasons. From top to bottom
835 the panels represent: DOC, a_{350}, $\delta^{13}C_{DOC}$, $SUVA_{254}$, S_R and FI. Dark gray and light gray
836 rectangles in background represent the approximate position along the mainstream of
837 wetlands/flooplains areas and reservoirs, respectively. Roman numerals refer to (I)
838 Barotse Floodplain, (II) Chobe Swamps, (III) Kariba Reservoir, (IV) Cahora Bassa
839 Reservoir, (V) lower Zambezi wetlands for the Zambezi River and (VI) Lukanga Swamps,
840 (VII) Itezhi Tezhi Reservoir and (VIII) Kafue Flats for the Kafue River. The diamonds
841 represent samples collected from main tributaries upstream of their confluence with
842 mainstreams: (IX) the Kabompo, (X) the Kafue, (XI) the Luangwa, (XII) the Mazoe and

(XIII) Shire River for the Zambezi River and (XIV) the Lunga River for the Kafue River. Symbols and error bars for data collected during the wet seasons represent the average and standard deviation between the two field campaigns performed in 2012 and 2013, respectively.

Figure 4 – Relationships between DOC and % wetlands in the catchement in the Zambezi and the Kafue rivers during the wet periods, with *:p<0.1, and ***:p<0.001. For the Zambezi, only the samples collected in the upper part of the basin have been considered due to the effect of the Kariba and Cahora Bassa reservoirs on the longitudinal pattern of DOC concentrations.

Figure 5 – Longitudinal variations of FDOM along the Zambezi River (left panels) and the Kafue River (right panels) during the wet and the dry seasons. From top to bottom the panels represent: F_{Tot} and F_{Max} for each PARAFAC component. The diamonds represent samples taken from main tributaries upstream of their confluence with mainstreams.

Figure 6 – Longitudinal variations of the relative contribution of PARAFAC component along the Zambezi River (left panels) and the Kafue River (right panels) during the wet and the dry seasons. The diamonds represent samples taken from main tributaries upstream of their confluence with mainstreams.

Figure 7 – Graphical representation of PCA results, including loadings plot for the input variables and scores plot for water samples collected during the wet (circles) and the dry (triangles) seasons. Water samples from the Zambezi River (ZBZ) were classified

867 according to its source and the three major segments of the Zambezi basin. Samples from
868 reservoirs (i.e. Kariba, Cahora Bassa and Itezhi Tezhi reservoirs) were classified together.
869
870 **Figure 8 –** DOC exports calculated at different locations along the Zambezi River during
871 the wet and the dry seasons. Vertical arrows represent changes in DOC exports at the
872 same location between wet and dry seasons. Diagonal changes represent longitudinal
873 variations.

Table 1– Spectral characteristics of the five fluorophores identified by PARAFAC modelling, correspondence with previously identified components in different environments, general assignment and possible source. Numbers in brackets refer to the second peak of maximal excitation.

Component	Maximum Excitation (nm)	Maximum Emission (nm)	Comparison with others environments								Assignement	Possible source[a]
			St Lawrence River[1]	Large Arctic rivers[2]	Boreal Lakes[3,4]	Subtropical wetlands[5,6]	Tropical wetland[7]	Temperate estuary[8]	Coastal waters[9]	Marine waters[10]		
C1	<240 (325)	443	C2	C1	C4	C1	C1	C4	—	C1	Terrestrial humic-like	T
C2	<240 (365)	517	C3	C3	C3	C5	C4	C2	C3	—	Terrestrial humic-like	T
C3	<240 (305)	383	C7	—	C2	C4	C3	C6	C6	C4	Microbial humic-like	Au[9],M[3,7,10], An[8]
C4	<240	405	C1	—	C5	C2	C2	C1	C1	—	Terrestrial humic-like	T[5-6,8], P[1,4]
C5	275 (<240)	337	C4	C5	C6	C8	—	C7	C4	C2	Tryptophan-like	Au[1,9], M[2,8]

[a] T: Terrestrial inputs; Au: Autochthonous primary production; An: Anthropogenic origin; M: Microbial degradation; P: Photochemical degradation.

1) Massicotte and Frenette (2011); 2) Walker et al. (2013); 3) Kothawala et al. (2014); 4) Kellerman et al. (2015); 5) Yamashita et al. (2010); 6) Cawley et al. (2012); 7) Zürbrugg et al. (2013); 8) Stedmon and Markager (2005); 9) Yamashita et al. (2008); 10) Jørgensen et al. (2011).

Table 2 – Temporal variations of DOM properties measured at the outlet of the Kariba Reservoir during an almost two-year monthly sampling (from February 2012 to November 2013).

	DOC (mg L^{-1})	$\delta^{13}C_{DOC}$ (‰)	a_{350} (m-1)	$SUVA_{254}$ (L mgC-1 m-1)	S_R	%C1	%C2	%C3	%C4	%C5
Min	2,00	-23,96	1,00	1,39	1,010	27,7	12,2	16,1	4,0	12,3
Max	2,60	-22,26	2,50	3,11	1,428	36,5	16,6	26,2	13,8	35,9
Mean	2,22	-23,08	1,60	2,02	1,185	34,1	15,2	24,1	9,3	17,3
S.D.	0,17	0,37	0,44	0,43	0,141	2,4	1,2	2,7	3,1	6,2
n	*20*	*20*	*12*	*12*	*12*	*12*	*12*	*12*	*12*	*12*

882 **Figure 1**

883

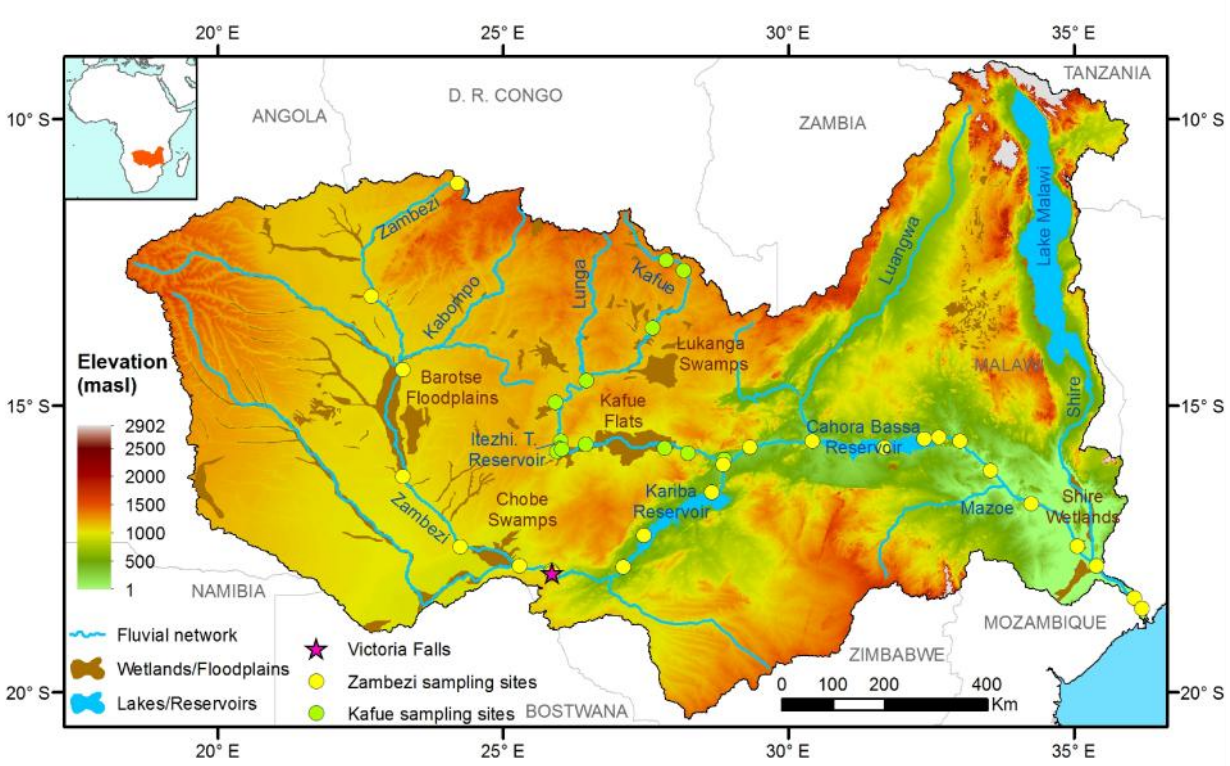

884

885 **Figure 2**

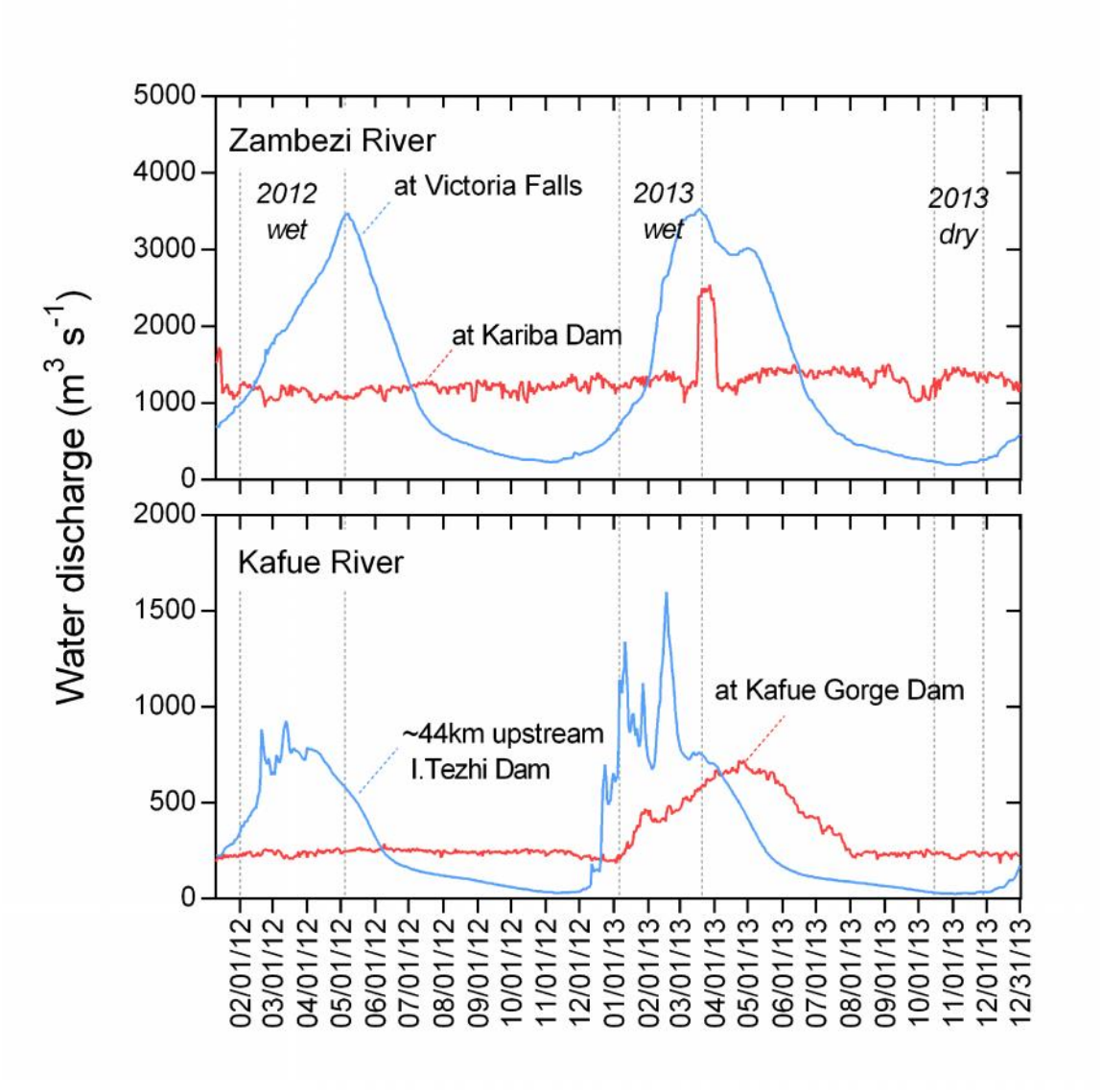

886

887 **Figure 3**

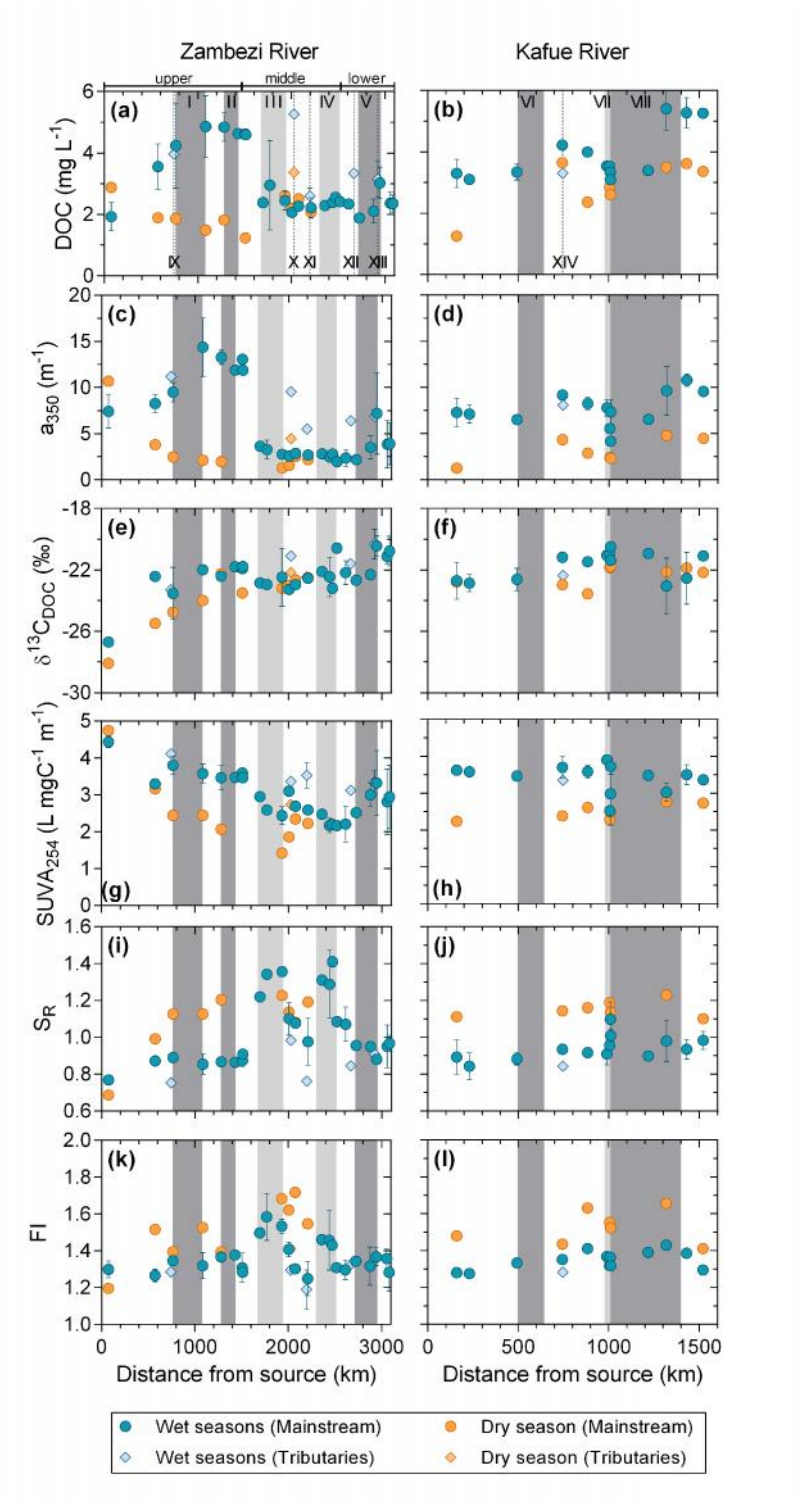

888

889 **Figure 4**

890

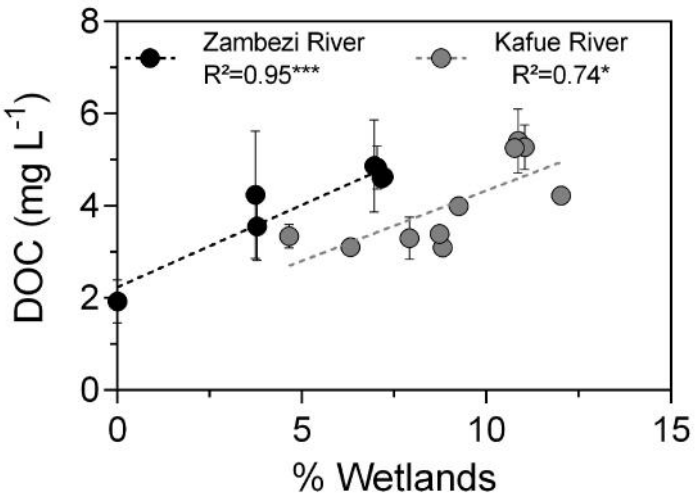

891

892 **Figure 5**

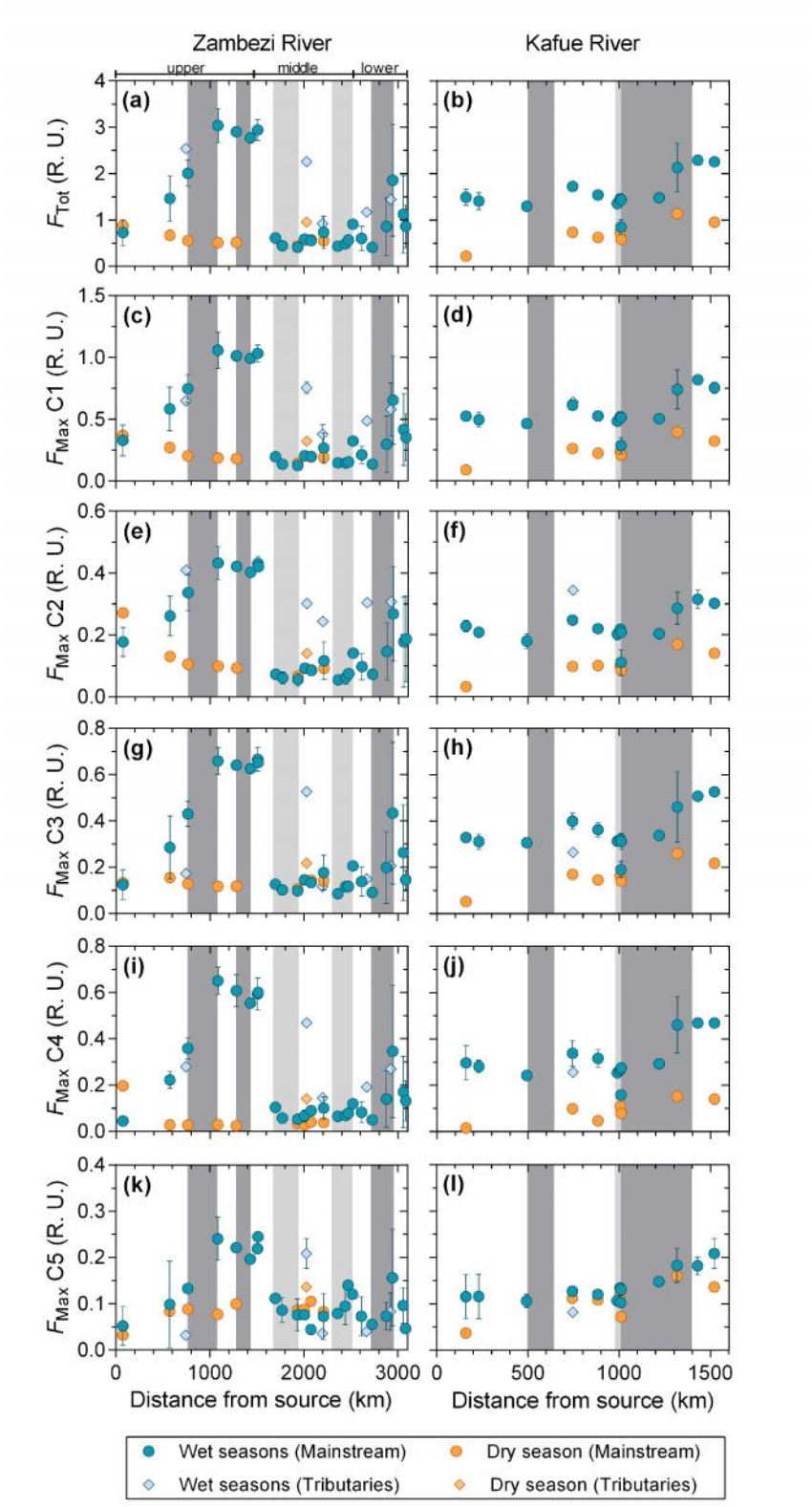

893

894 **Figure 6**

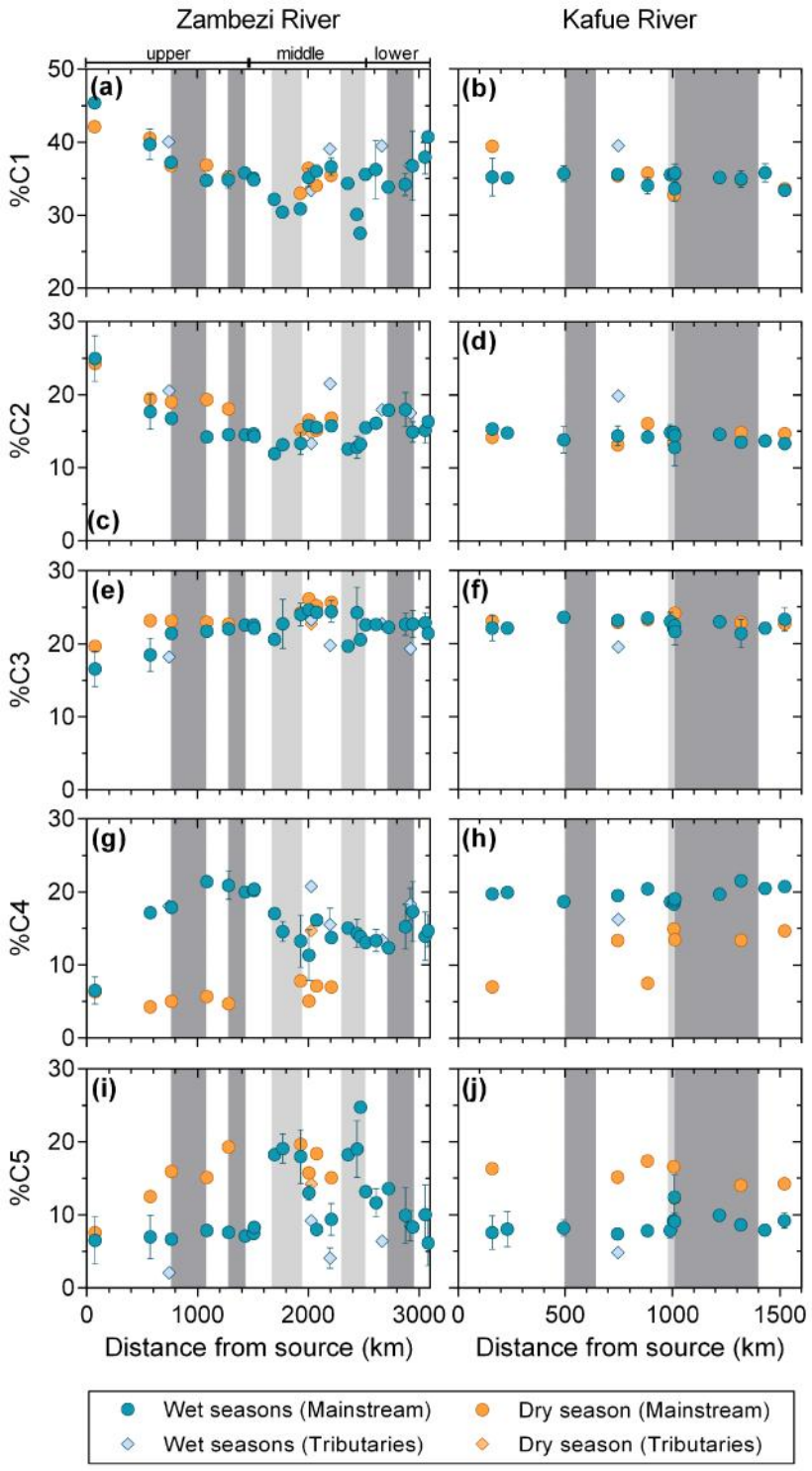

895

Figure 7

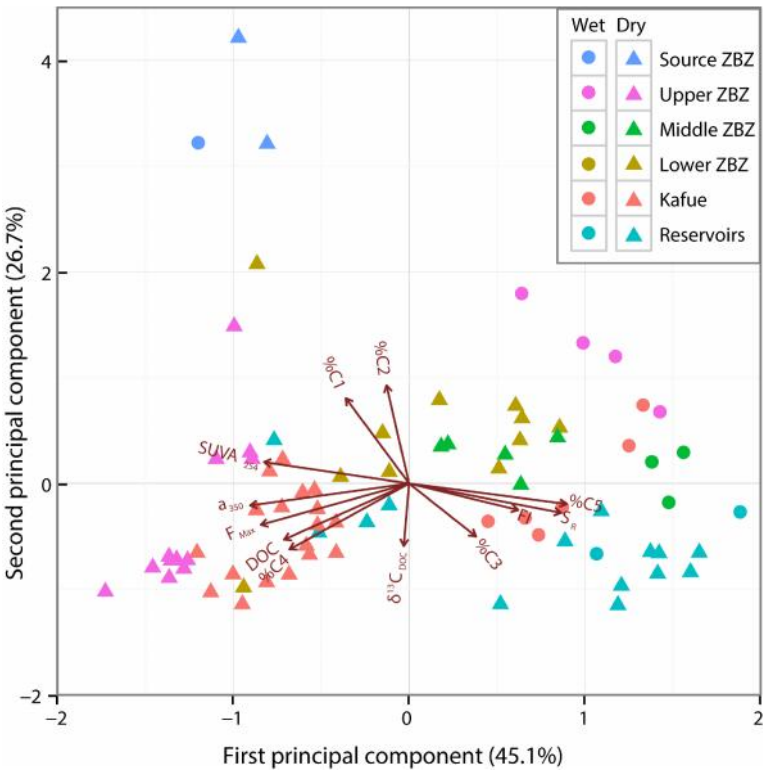
Wet Dry
Source ZBZ
Upper ZBZ
Middle ZBZ
Lower ZBZ
Kafue
Reservoirs
%C1
%C2
%C3
%C4
%C5
%C6
SUVA254
a350
FMax
DOC
SR
FI
Second principal component (26.7%)
First principal component (45.1%)
4
2
0
−2
−2
−1
0
1
2

898 **Figure 8**

899

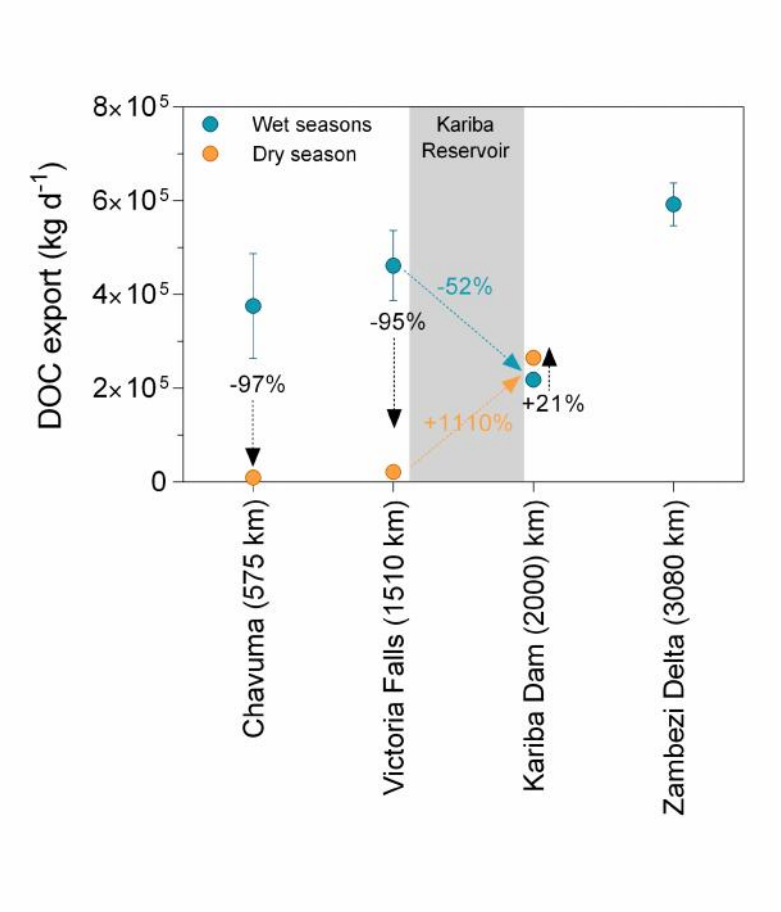

900

901

902